IEEE Photonics Journal
An IEEE Photonics Society Publication

Experimental Investigation of Iterative Pseudoinverse Ghost Imaging

Volume 10, Number 3, June 2018

Xiaofeng Lv
Shuxu Guo
Chenglong Wang
Chao Yang
Hongwei Zhang
Junfeng Song
Wenlin Gong
Fengli Gao

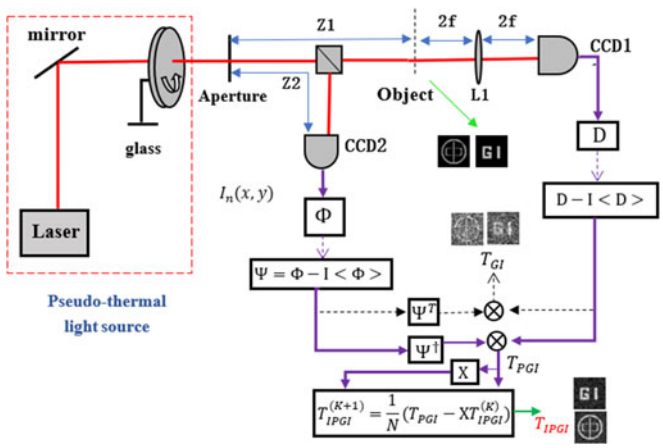

DOI: 10.1109/JPHOT.2018.2832720
1943-0655 © 2018 IEEE

Experimental Investigation of Iterative Pseudoinverse Ghost Imaging

Xiaofeng Lv,[1] **Shuxu Guo**,[1] **Chenglong Wang**,[2] **Chao Yang**,[1] **Hongwei Zhang**,[1] **Junfeng Song**,[1] **Wenlin Gong**,[2] **and Fengli Gao** [1]

[1]State Key Laboratory on Integrated Optoelectronics, College of Electronic Science and Engineering, Jilin University, Changchun 130012, China
[2]Key Laboratory for Quantum Optics and Center for Cold Atom Physics, Shanghai Institute of Optics and Fine Mechanics, Chinese Academy of Sciences, Shanghai 201800, China

DOI:10.1109/JPHOT.2018.2832720

Manuscript received April 19, 2018; accepted April 30, 2018. Date of publication May 7, 2017; date of current version May 23, 2018. This work was supported in part by the National Key Research and Development Program of China under Grant 2016YFE0200700, in part by the Natural Science Foundation of the Science and Technology Development Program of the Jilin Province, China, under Grant 20160101284JC, in part by the National Natural Science Foundation of China under Grant 61571427, in part by the Youth Innovation Promotion Association of the Chinese Academy of Sciences, and in part by the Open Foundation of State Key Laboratory of Luminescence and Applications, China, under Grant SKLA-2016-05. Corresponding authors: Wenlin Gong and Fengli Gao (e-mail: gongwl@siom.ac.cn; gaofl@jlu.edu.cn).

Abstract: An iterative pseudoinverse ghost imaging (IPGI) method is proposed based on iterative denoising and pseudoinverse ghost imaging (PGI). The background noise in the imaging is eliminated in iterations by setting an appropriate threshold. The IPGI method provides a significantly larger enhancement of the peak signal-to-noise ratio (PSNR) than the PGI technique for binary objects. Experiments and data analyses are performed to evaluate the performance of the proposed method. Compared with conventional GI, differential GI, and PGI methods, the proposed method has the highest performance in visual effects and significantly improves the imaging quality. For a certain PSNR, the proposed method provides satisfactory performance in terms of computing time.

Index Terms: Imaging processing, coherence imaging, photon statistics, quantum optics.

1. Introduction

Ghost imaging (GI), which achieves the separation of imaging and detection, is a nonlocal imaging technique. In a GI system, the light field through a beam splitter is divided into two beams with spatial correlation: object beam, modulated by the unknown object and collected by a bucket detector, and reference beam, which after propagating a certain distance is directly recorded by the detector with spatial resolution. By calculating the second-order correlation function between the bucket signal and known light patterns from the reference beam, the object image can be retrieved. The GI technique was originally implemented employing entangled photon pairs generated by spontaneous parametric down-conversion (SPDC) [1]. Subsequently, numerous theoretical and experimental studies have demonstrated that pseudo-thermal light and thermal light [2] could be also used, which has accelerated the progress of GI from laboratory to practical applications. Based on these features, GI, which is based on the entangled nature of two-phonon or classical intensity-fluctuation correlations, has been extensively studied [3]–[8]. It has been employed in

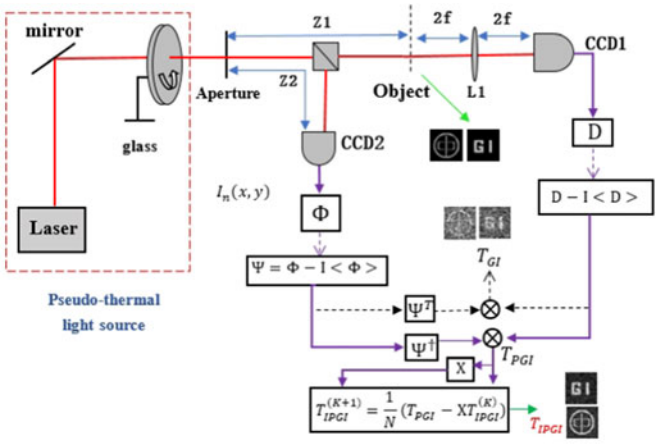

Fig. 1. Setup of the IPGI. The distance f is the focal length of L1, Z1 represents the distance from the object to the pseudo-thermal source, and Z2 denotes the distance from the CCD2 to the pseudo-thermal light source (equal to Z1). In the bottom of the schematic, the dotted line represents the traditional GI reconstruction process, while the solid line represents the IPGI reconstruction process.

optical encryption [9], [10], remote sensing [11], lidar detection [12]–[15], etc. However, the poor visibility and large measurement time in GI have hindered real applications; therefore, improvements of the image quality and imaging efficiency are required.

In recent years, in order to overcome these challenges, various modified methods, including differential ghost imaging (DGI) [16], [17], pseudo-inverse ghost imaging (PGI) [18], [19], compressive ghost imaging [20], [21], and other methods [22]– [25], have been proposed and demonstrated. The DGI method utilizes a differential bucket signal factor to weight the speckle patterns for each measurement, which can significantly enhance the signal–to–noise ratio (SNR) and improve the order of magnitude depending on the object's absorbing property [17]. Iterative denoising of ghost imaging [23] provides significantly better performance than that of DGI; however, reconstruction results with a good SNR require a large number of measurements. Based on the target sparsity or compressibility, compressive GI can produce a better SNR, significantly below the Nyquist sampling frequency at the cost of a larger computation time [20], [21]. Using the property of the pseudo-inverse matrix, PGI was proposed and implemented [18], [19], [26]. Compared with the previous algorithms, it could provide a larger enhancement of the spatial resolution with less acquisition data and smaller computation time.

In this study, by combining the advantages of the PGI method and iterative denoising, we propose an iterative pseudo-inverse ghost imaging (IPGI) technique to further eliminate the background noise in the reconstructed results. Compared to GI and DGI, the proposed technique improves the image quality and reconstructs an N-pixel image from significantly less than N measurements. The experiments indicate that the IPGI technique exhibits better performance in the enhancement of the peak-signal–to–noise ratio (PSNR) than PGI, and significantly better performance than DGI for a binary object. Accordingly, IPGI advances the theoretical formalism for real applications of the GI method.

2. Experimental Setup and Theoretical Method

The schematic of the experimental setup with a pseudo-thermal source is shown in Fig. 1. The pseudo-thermal light source is generated from a laser beam at $\lambda = 532$ nm through a rotating ground glass, and then passes through an aperture to adjust the speckle size of the random speckle field. A polarization beam splitter (50:50) is then used to separate the beam into two different optical imaging paths: object path and reference path. At the object path, the transmitted or reflected light beam passing through the object with a transmission coefficient of $T(x, y)$ is recorded by a bucket

detector (summing the intensities of all of the pixels of a charge-coupled device (CCD1)); the *nth* measurement bucket signal is denoted as D_n. The reference beam, after propagating a certain distance in the free space, is directly collected by a CCD2 with spatial resolution; the *nth* acquisition intensity distribution signal is recorded as $I_n(x, y)$.

In the conventional GI, by correlating the total light intensity D_n and speckle pattern intensity distribution $I_n(x, y)$ to illumine the surface of the object, the imaging object can be deduced. Therefore, the mathematical form of the GI reconstruction formula is expressed as:

$$T_{GI}(x, y) = \frac{1}{N}\sum_{n=1}^{N}(D_n - \langle D_n\rangle)(I_n - \langle I_n\rangle) \tag{1}$$

where $\langle D_n\rangle = 1/N\sum_{n=1}^{N} D_n$ denotes the ensemble average of the total light intensity; similarly, $\langle I_n(x, y)\rangle = 1/N\sum_{n=1}^{N} I_n(x, y)$ denotes the ensemble mean at each pixel in N measurements.

To facilitate the analysis, Eq. (1) is transformed into a series of matrix operations. Assuming that the transmission function of the object $T(x, y)$ is a $q \times q$ matrix, and that the speckle pattern $I_n(x, y)$ detected by the reference camera (CCD2) is a matrix with the same size as that of T, Eq. (1) can be expressed in matrix form as:

$$\boldsymbol{T}_{GI} = \frac{1}{N}(\Phi - \boldsymbol{I}\ \langle\Phi\rangle)^T(\boldsymbol{D} - \boldsymbol{I}\ \langle\boldsymbol{D}\rangle) \tag{2}$$

In Eq. (2), the speckle pattern at the reference path is rearranged in an M-dimensional ($M = q\times q$) row vector to form one row of the matrix Φ for each realization. After N realizations, we obtain a matrix Φ with a size of $N\times M$, where $\langle\Phi\rangle$ denotes a $1\times M$ row vector consisting of the mean of each pixel for all of the N measurements, and $\boldsymbol{I}$ denotes an $N\times 1$ column vector whose elements are equal to 1; $\Psi = (\Phi - \boldsymbol{I}\ \langle\Phi\rangle)$ can be expressed as:

$$\Psi = (\Phi - \boldsymbol{I}\ \langle\Phi\rangle) = \begin{bmatrix} I_1(1,1) & I_1(1,2) & \cdots & I_1(q,q) \\ I_2(1,1) & I_2(1,2) & \cdots & I_2(q,q) \\ \vdots & \vdots & \ddots & \vdots \\ I_N(1,1) & I_N(1,2) & \cdots & I_N(q,q) \end{bmatrix} - \boldsymbol{I}\begin{bmatrix} \langle I_n(1,1)\rangle \\ \langle I_n(1,2)\rangle \\ \vdots \\ \langle I_n(q,q)\rangle \end{bmatrix}^T \tag{3}$$

Similarly, $\boldsymbol{D} = [D_1, D_2, D_3\cdots\cdots D_N]^T$ consists of the bucket signals at the object path, and $\langle\boldsymbol{D}\rangle$ represents the ensemble average of the vector $\boldsymbol{D}$. Simultaneously, the transmission function of the object $T(x, y)$ is permutated into a $q^2 \times 1$ column vector $\boldsymbol{T}$. As $D_n = \int\int I_n(x, y)T(x, y)dxdy$, $\boldsymbol{D} - \boldsymbol{I}\ \langle\boldsymbol{D}\rangle$ can be converted to $(\Phi - \boldsymbol{I}\ \langle\Phi\rangle)\boldsymbol{T}$. Therefore, the GI formula can be expressed as:

$$\boldsymbol{T}_{GI} = \frac{1}{N}(\Phi - \boldsymbol{I}\ \langle\Phi\rangle)^T(\Phi - \boldsymbol{I}\ \langle\Phi\rangle)\boldsymbol{T} = \frac{1}{N}\Psi^T\Psi\boldsymbol{T} \tag{4}$$

However, in the DGI method, the speckle field is weighed by a modified differential bucket signal for each measurement, where fluctuations of the weight factor can emerge mainly from the relative change in the object's transmission function. The DGI reconstruction can be expressed as:

$$\boldsymbol{T}_{DGI} = \frac{1}{N}(\Phi - \boldsymbol{I}\ \langle\Phi\rangle)^T\left(\boldsymbol{D} - \frac{\langle\boldsymbol{D}\rangle}{\langle\boldsymbol{E}\rangle}\boldsymbol{E}\right) \tag{5}$$

where $\boldsymbol{E} = [E_1, E_2, E_3, \cdots\cdots E_N]^T$, $\boldsymbol{E}_n$ is a sum of the reference signals in *nth* measurements, and $\langle\boldsymbol{E}\rangle$ denotes the ensemble mean of the total intensity calculated by the reference CCD2 in N measurements. It is known that the change of the bucket signals is triggered by the overlap of the known light pattern with the object, hence the reconstruction can be also expressed as:

$$\boldsymbol{T}_{DGI} = \frac{1}{N}(\Phi - \boldsymbol{I}\ \langle\Phi\rangle)^T(\Phi - \boldsymbol{I}\ \langle\Phi\rangle)\Delta\boldsymbol{T} = \frac{1}{N}\Psi^T\Psi(\boldsymbol{T} - \overline{\boldsymbol{T}}) \tag{6}$$

where $\Delta\boldsymbol{T} = \boldsymbol{T} - \overline{\boldsymbol{T}}$ represents the relative difference between the transmission function of the object and average transmission function.

In the PGI technique, the pseudo-inverse matrix ($\Psi^{\dagger}$) of Ψ is obtained using the Moore–Penrose equation. Instead of Ψ^{T}, the imaging object is retrieved by measuring the intensity-fluctuation correlations between $\Psi^{\dagger}$ and $\boldsymbol{D}$. The PGI can be expressed as:

$$\boldsymbol{T}_{\mathrm{PGI}} = \frac{1}{N}\Psi^{\dagger}\Psi\boldsymbol{T} \tag{7}$$

where the matrix $\Psi^{\dagger}\Psi$ can be divided into two matrices: $\boldsymbol{s} = \mathrm{diag}(\Psi^{\dagger}\Psi)$, which is composed of all of the diagonal elements and contains effective information of the reconstruction, and $\boldsymbol{n} = \Psi^{\dagger}\Psi - \boldsymbol{s}$, which consists of all of the non-diagonal elements, and represents a noise disturbance term. Theoretically, when $\boldsymbol{s}$ is closer to a scalar matrix, and $\boldsymbol{n}$ is similar to the matrix whose elements are zero, $\boldsymbol{T}_{\mathrm{PGI}}$ will be more proximate to the original image of the object. Therefore, the process of decomposition and reconstruction is described as:

$$\Psi^{\dagger}\Psi = \boldsymbol{s} + \boldsymbol{n} \tag{8}$$

$$\boldsymbol{T}_{\mathrm{PGI}} = \frac{1}{N}\Psi^{\dagger}\Psi\boldsymbol{T} = \frac{1}{N}\boldsymbol{s}\boldsymbol{T} + \frac{1}{N}\boldsymbol{n}\boldsymbol{T} \tag{9}$$

Based on the above analysis, $(1/N)\boldsymbol{n}\boldsymbol{T}$ is the actual noise in the PGI reconstruction, whose presence obscures the image. Without prior information of the object, the PGI reconstruction results are used as initial values to construct the hypothetical noise interference $(1/N)\boldsymbol{n}'\boldsymbol{T}_{\mathrm{PGI}}$, aiming to approximate the actual noise; then, $(1/N)\boldsymbol{n}'\boldsymbol{T}_{\mathrm{PGI}}$ is subtracted from Eq. (9) in order to better suppress the noise; this method is referred to as denoising PGI (DPGI). The denoising process can be described as:

$$\boldsymbol{T}_{DPGI} = \frac{1}{N}\boldsymbol{s}\boldsymbol{T} + \frac{1}{N}\boldsymbol{n}\boldsymbol{T} - \frac{1}{N}\boldsymbol{n}'\boldsymbol{T}_{\mathrm{PGI}} \tag{10}$$

$$n'(x,y) = \begin{cases} n(x,y) & n(x,y) \le t \\ 0 & n(x,y) > t \end{cases} \tag{11}$$

where the threshold t is used to retain or clear some of the location information in $n'(x,y)$. Therefore, the more effective information is retained in the reconstruction; the noise can also be well-suppressed when we choose the appropriate threshold t. Based on the character of the iterative denoising, we consider the use of iterative algorithms to further eliminate the actual noise in the PGI, referred to as an IPGI method, defined as:

$$\boldsymbol{T}_{IPGI}^{(K+1)} = \frac{1}{N}\Psi^{\dagger}\Psi\boldsymbol{T} - \frac{1}{N}\boldsymbol{X}\boldsymbol{T}_{IPGI}^{(K)} \tag{12}$$

where $\boldsymbol{T}_{IPGI}^{(0)} = \boldsymbol{T}_{\mathrm{PGI}}$, $\boldsymbol{T}_{IPGI}^{(1)} = \boldsymbol{T}_{DPGI}$, $\boldsymbol{X} = \Psi^{\dagger}\Psi - \mathrm{diag}(\Psi^{\dagger}\Psi)$ ($\mathrm{diag}(\cdot)$ denotes matrix diagonal elements), and $X(x,y)$ is set to zero when $X(x,y)$ is larger than the threshold t; otherwise, the value is retained. As the threshold t varies from $\min\{n(x,y)\}$ to $\max\{n(x,y)\}$ in the experiment, a normalized threshold $t' = \frac{t-\min\{n(x,y)\}}{\max\{n(x,y)\}-\min\{n(x,y)\}}$ is utilized to simplify the experimental analysis. During the iteration process of the IPGI, the original image retrieved within the PGI as an initial value is employed for the IPGI iterative formula, leading to a better image. By repeating the above steps, the reconstruction results become closer to the original object. This iterative process can be repeated K times until the PSNR reaches the maximum value to obtain the final IPGI image. In our experiments, we verified that the PSNR of the IPGI reaches the maximum value for a number of iterations of only $K = 3$.

3. Experimental Results

We verify the validity of the IPGI using the experimental setup illustrated in Fig. 1, where the distance Z1 between the object plane and pseudo-thermal source (Z1 = Z2) is 200 mm, the focal length f of the lens L1 is 150 mm, and the distance between the CCD1 and lens L1 is $2f = 300$ mm. CCD1 is identical to CCD2; however, CCD1 is used as a bucket detector collecting the total light intensity of all pixels. In addition, the speckle transverse size on the object plane is changed by adjusting the

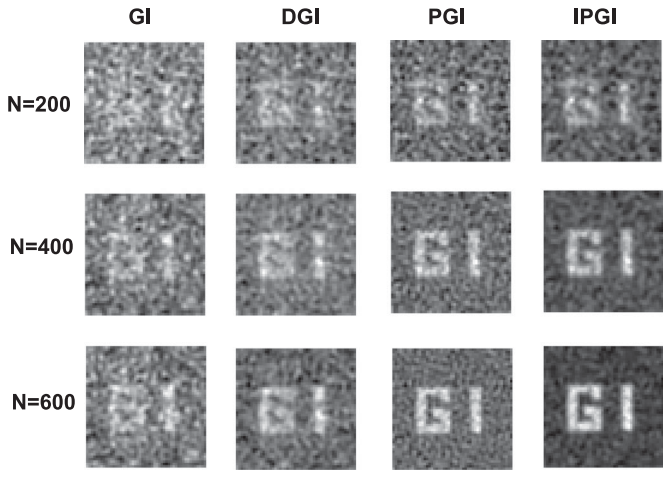

Fig. 2. Comparison of the experimental results of GI, DGI, PGI, and IPGI, as a function of the number of measurements; the results for 200, 400, and 600 measurements are shown in the top, middle, and bottom panels, respectively.

aperture. In the experiments, first, we select a binary transmission aperture "GI" with 50 $\times$ 50 pixels as a reconstructed object; the speckle transverse size is approximately 17$\times$17 pixels, with respect to the pixel size of the CCD camera (Stingray F-504B, AVT, Germany). The reconstruction results of the GI, DGI, and PGI are compared with those of IPGI under the conditions of a normalized threshold of $t' = 0.4$ and number of iterations of $K = 3$; the reconstruction results are shown in Fig. 2.

Fig. 2 reveals that the visual effects of all of the reconstructions are enhanced with the increase of the number of measurements N. For a certain number of measurements, GI performs poorly; its retrieved images are almost covered by background noise. The results of DGI are relatively improved; however, significant noise still exists. Compared with GI and DGI, the PGI reconstructions can improve the imaging resolution and provide sharp edges; IPGI can provide a significantly larger improvement in the visual effects than PGI. In addition, the contrast of the images is significantly enhanced using IPGI, compared with the PGI method. The experiments show that the IPGI method can better suppress the background noise.

In the experiment, PSNR is introduced to estimate the reconstruction fidelity and quantitatively compare the qualities of reconstruction for different methods; PSNR is defined as:

$$\mathrm{PSNR} = 10 \times 10 \log_{10}^{\left[\frac{2^m - 1}{MSE}\right]} \tag{13}$$

where $m = 8$ for an image with grayscale in the range of 0 to 255; MSE denotes the mean square error between the original image and retrieved image. A higher PSNR implies a better fidelity of the reconstructed image. The PSNR results are shown in Fig. 3.

The construction results in Fig. 2 correspond to the PSNR curves in Fig. 3. Fig. 3 shows that, overall, all of the PSNRs tend to increase with the number of measurements N (from 100 to 600). For a binary transmission aperture, the PSNR of the IPGI is larger than those of the other methods for the same number of measurements. In addition, the PGI method is superior with respect to the DGI method. For 600 measurements, the PSNR of the IPGI is approximately 14.2 dB, which is 4.1 dB, 4.3 dB, and 6.2 dB higher than those of the PGI, DGI, and conventional GI methods, respectively. The visual effects and quantitative results in Figs. 2 and 3, respectively, are consistent. The above experimental results preliminarily demonstrate that IPGI can significantly improve the PSNR of the reconstructed image.

In order to further verify the effectiveness of the IPGI method for other general binary images with different sparsities and speckle sizes, experiment results for another object "Zhong" (50$\times$50 pixels)

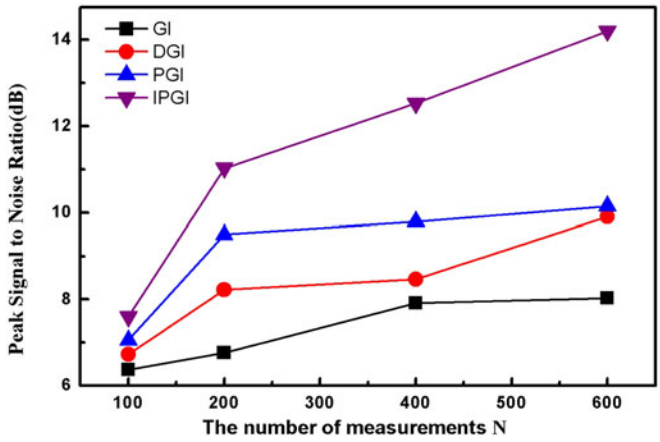

Fig. 3. PSNR curves for GI, DGI, PGI, and IPGI as a function of the number of measurements.

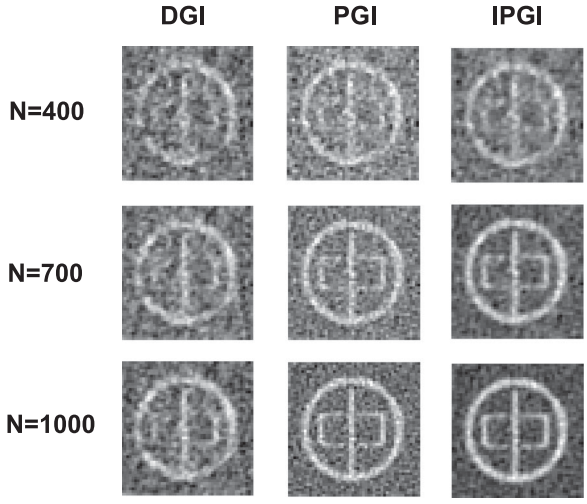

Fig. 4. Experimental results for the "Zhong" object obtained by the DGI (left column), PGI (middle column), and IPGI (right column) methods for 400, 700, and 1000 measurements.

obtained by the three methods (DGI, PGI, and IPGI) for numbers of measurements of 400, 700, and 1,000 are shown in Fig. 4. The experimental parameters are consistent with those in Fig. 2, except that the speckle transverse size on the object plane is approximately 11×11 pixels, with respect to the pixel size of the CCD. The experimental results in Fig. 4 are similar to those in Fig. 2 in the visual effects, which further confirms the effectiveness of the IPGI method and its advantage in the enhancement of the imaging quality.

The computing time is one of the important indicators to evaluate the merits of a method. Therefore, we record the imaging times of DGI, PGI, and IPGI for different numbers of measurements (computer configuration: Intel(R) Xeon(R) CPU E5-1650V4, 3.6 GHz; RAM: 64.0 GB). The results for the "GI" object are shown in Fig. 5. In general, Fig. 5 shows that the computing time almost linearly increases with the number of measurements N; the time costs of the DGI and PGI methods are comparable. Although the reconstruction time of IPGI is larger than that of the other methods for a given number of measurements, Figs. 3 and 5 show that, for certain PSNR or imaging quality (such as the results of IPGI at $N = 200$ and PGI at $N = 600$), the IPGI method requires less measurements than the PGI method; therefore, its computing time is smaller than that of the PGI method. In summary, for transmissive objects, the PSNR of the imaging object can be significantly improved by the IPGI method at the expense of the computing time.

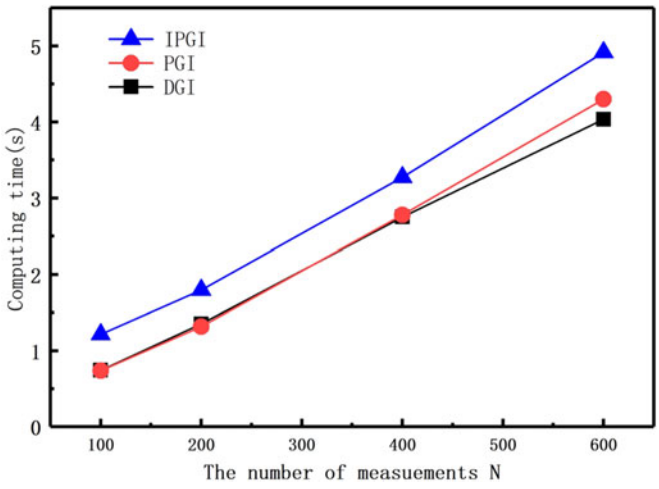

Fig. 5. Comparison of the computing times of the DGI, PGI, and IPGI methods for the "GI" object for different numbers of measurements N.

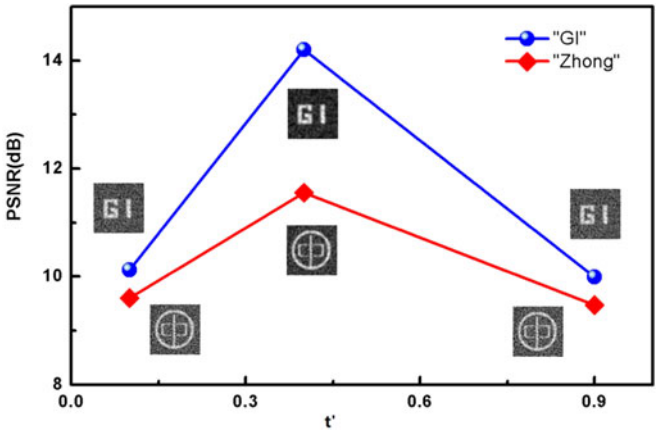

Fig. 6. Experimental results and PSNR curves of IPGI as a function of the threshold t'. The numbers of measurements N for the "Zhong" and "GI" objects are 1,000 and 600, respectively. For both curves, the first, second, and third points correspond to t' of 0.1, 0.4, and 0.9, respectively.

Numerical and theoretical results indicated that the selection of a proper threshold is crucial for the quality of the reconstructed image; therefore, considering the impact of the normalized threshold t' on the IPGI results, the reconstruction results and PSNR curves as a function of the threshold t' are presented in Fig. 6, where the insets show the corresponding reconstructed images.

Fig. 6 shows that the IPGI result with a low threshold has a degraded quality; the performance of the IPGI with a high threshold is close to that for the low threshold. However, the reconstruction with a proper threshold yields better quality and PSNR; the inset pictures reveal that the imaging noise is well suppressed at a threshold of $t' = 0.4$. Therefore, the IPGI method with a proper threshold can further reduce the noise influence and improve the PSNR of the retrieved images; $t' = 0.4$ is equal to that reported in a previous study [23].

4. Conclusion

In conclusion, we have proposed an IPGI method to obtain reconstructed images with a high PSNR, even for cases significantly below the Nyquist limit. During the iterative process, the retrieved image

of the PGI is used as an initial value, the background noise and reconstructed image are continuously updated, and finally, a better image is obtained. Compared with the GI, DGI, and PGI methods, the experimental results indicate that the proposed method is effective for the enhancement of the visual effects and PSNR of the reconstructed images. In addition, the time performances of the DGI, PGI, and IPGI methods are analyzed and compared. The IPGI method can obtain the same imaging quality as those of DGI and PGI with a lower time cost. Therefore, in the experiments with a properly selected threshold, the proposed method can achieve a better performance than those of the PGI and DGI methods for a binary object. In addition, a threshold selection based on an iterative algorithm is of interest in our future research. We believe that the proposed technique contributes to the GI for applications in various fields.

References

[1] T. B. Pittman, Y. H. Shih, D. V. Strekalov, and A. V. Sergienko, "Optical imaging by means of two-photon quantum entanglement," *Phys. Rev. A*, vol. 52, no. 5, pp. R3429–R3432, 1995.

[2] P. Zerom *et al.*, "Thermal ghost imaging with averaged speckle patterns," *Phys. Rev. A*, vol. 86, no. 6, 2012, Art. no. 063817.

[3] R. S. Bennink, S. J. Bentley, and R. W. Boyd, ""Two-photon"" coincidence imaging with a classical source," *Phys. Rev. Lett.*, vol. 89, no. 11, 2002, Art. no. 113601.

[4] A. Gatti, E. Brambilla, M. Bache, and L. A. Lugiato, "Ghost imaging with thermal light: Comparing entanglement and classical correlation," *Phys. Rev. Lett.*, vol. 93, no. 9, 2004, Art. no. 093602.

[5] J. Cheng and S. S. Han, "Incoherent coincidence imaging and its applicability in x-ray diffraction," *Phys. Rev. Lett.*, vol. 92, no. 9, 2004, Art. no. 093903.

[6] J. H. Shapiro and R. W. Boyd, "The physics of ghost imaging," *Quantum Inf. Process.*, vol. 11, no. 4, pp. 949–993, 2012.

[7] R. Meyers, K. S. Deacon, and Y. Shih, "Ghost-imaging experiment by measuring reflected photons," *Phys. Rev. A*, vol. 77, no. 4, 2008, Art. no. 041801.

[8] W. L. Gong and S. S. Han, "The influence of axial correlation depth of light field on lensless ghost imaging," *J. Opt. Soc. Amer. B*, vol. 27, no. 4, pp. 675–678, 2010.

[9] P. Clemente, V. Duran, V. Torres-Company, E. Tajahuerce, and J. Lancis, "Optical encryption based on computational ghost imaging," *Opt. Lett.*, vol. 35, no. 14, pp. 2391–2393, 2010.

[10] S. Yuan, X. M. Liu, X. Zhou, and Z. Y. Li, "Optical encryption scheme with multiple users based on computational ghost imaging and orthogonal modulation," *J. Opt. Soc. Korea*, vol. 20, no. 4, pp. 476–480, 2016.

[11] B. I. Erkmen, "Computational ghost imaging for remote sensing," *J. Opt. Soc. Amer. A*, vol. 29, no. 5, pp. 782–789, 2012.

[12] C. Q. Zhao *et al.*, "Ghost imaging lidar via sparsity constraints," *Appl. Phys. Lett.*, vol. 101, no. 14, 2012, Art. no. 141123.

[13] H. Yu, E. R. Li, W. L. Gong, and S. S. Han, "Structured image reconstruction for three-dimensional ghost imaging lidar," *Opt. Exp.*, vol. 23, no. 11, pp. 14541–14551, 2015.

[14] W. L. Gong, C. Q. Zhao, H. Yu, M. L. Chen, W. D. Xu, and S. S. Han, "Three-dimensional ghost imaging lidar via sparsity constraint," *Sci. Rep.*, vol. 6, 2016, Art. no. 26133.

[15] C. J. Deng, L. Pan, C. L. Wang, X. Gao, W. L. Gong, and S. S. Han, "Performance analysis of ghost imaging lidar in background light environment," *Photon. Res.*, vol. 5, no. 5, pp. 431–435, 2017.

[16] W. L. Gong, and S. S. Han, "A method to improve the visibility of ghost images obtained by thermal light," *Phys. Lett. A*, vol. 374, no. 8, pp. 1005–1008, 2010.

[17] F. Ferri, D. Magatti, L. A. Lugiato, and A. Gatti, "Differential ghost imaging " *Phys. Rev. Lett.*, vol. 105, no. 21, 2010, Art. no. 219902.

[18] C. Zhang, S. X. Guo, J. S. Cao, J. Guan, and F. L. Gao, "Object reconstitution using pseudo-inverse for ghost imaging," *Opt. Exp.*, vol. 22, no. 24, pp. 30063–30073, 2014.

[19] W. L. Gong, "High-resolution pseudo-inverse ghost imaging," *Photon. Res.*, vol. 3, no. 5, pp. 234–237, 2015.

[20] O. Katz, Y. Bromberg, and Y. Silberberg, "Compressive ghost imaging," *Appl. Phys. Lett.*, vol. 95, no. 13, 2009, Art. no. 131110.

[21] J. Du, W. L. Gong, and S. S. Han, "The influence of sparsity property of images on ghost imaging with thermal light," *Opt. Lett.*, vol. 37, no. 6, pp. 1067–1069, 2012.

[22] C. Yang *et al.*, "Scalar-matrix-structured ghost imaging," *Photon. Res.*, vol. 4, no. 6, pp. 281–285, 2016.

[23] X. R. Yao *et al.*, "Iterative denoising of ghost imaging," *Opt. Exp.*, vol. 22, no. 20, pp. 24268–24275, 2014.

[24] W. Wang, Y. P. Wang, J. H. Li, X. X. Yang, and Y. Wu, "Iterative ghost imaging," *Opt. Lett.*, vol. 39, no. 17, pp. 5150–5153, 2014.

[25] B. Q. Sun, S. S. Welsh, M. P. Edgar, J. H. Shapiro, and M. J. Padgett, "Normalized ghost imaging," *Opt. Exp.*, vol. 20, no. 15, pp. 16892–16901, 2012.

[26] S. Chountasis, V. N. Katsikis, and D. Pappas, "Digital image reconstruction in the spectral domain utilizing the Moore-Penrose inverse," *Math. Probl. Eng.*, vol. 2010, 2010, Art. no. 750352.